energies

MDPI

Article

Performance and Design Optimization of a One-Axis Multiple Positions Sun-Tracked V-trough for Photovoltaic Applications

Guihua Li, Jingjing Tang and Runsheng Tang *

Education Ministry Key Laboratory of Advanced Technology and Preparation for Renewable Energy Materials, Yunnan Normal University, Kunming 650500, China; guihuali688@163.com (G.L.); jjtang166@126.com (J.T.)

* Correspondence: kingtang01@126.com

Received: 12 January 2019; Accepted: 18 March 2019; Published: 23 March 2019

Abstract: In this article, the performance of an inclined north-south axis (INSA) multiple positions sun-tracked V-trough with restricted reflections for photovoltaic applications (MP-VPVs) is investigated theoretically based on the imaging principle of mirrors, solar geometry, vector algebra and three-dimensional radiation transfer. For such a V-trough photovoltaic module, all incident radiation within the angle θ_a arrives on solar cells after less than k reflections, and the azimuth angle of V-trough is daily adjusted M times about INSA to ensure incident solar rays always within θ_a in a day. Calculations and analysis show that two-dimensional sky diffuse radiation can't reasonably estimate sky diffuse radiation collected by fixed inclined north-south V-trough, but can for MP-VPVs. Results indicate that, the annual power output (P_a) of MP-VPVs in a site is sensitive to the geometry of V-trough and wall reflectivity (ρ), hence given M, k and ρ, a set of optimal θ_a and φ, the opening angle of V-trough, for maximizing P_a can be found. Calculation results show that the optimal θ_a is about 21°, 13.5° and 10° for 3P-, 5P- and 7P-VPV-k/θ_a (k = 1 and 2), respectively, and the optimal φ for maximizing P_a is about 30° for k = 1 and 21° for k = 2when $\rho > 0.8$. As compared to similar fixed south-facing PV panels, the increase of annual electricity from MP-VPVs is even larger than the geometric concentration of V-trough for $\rho > 0.8$ in sites with abundant solar resources, thus attractive for water pumping due to stable power output in a day.

Keywords: V-trough with restricted reflections; one-axis multiple positions sun-tracking; three dimensional radiation transfer; performance investigation; design optimization

1. Introduction

Energy is essential for the daily life of human beings, but extensive use and exploitation has resulted in severe environmental and ecological consequences, hence direct use of solar energy for electricity and heat generation is becoming more attractive. In recent years, low temperature solar thermal techniques have been widely used for water and building heating, but applications of photovoltaic technology are limited due to the high cost of electricity from PV systems although the cost of solar cells has decreased dramatically in recent years [1–3]. Potential ways to reduce the cost of electricity from a PV system include the use of sun-tracking techniques and cheap optical concentrators. Continuous sun-tracking can increase the power output from PV systems, but sophisticated sun-tracking and control devices are required [4]. In recent years, low concentrators such as compound parabolic concentrators (CPCs) and V-trough concentrators have been widely tested for concentrating radiation on solar cells. Compared with similar PV panels, a low concentrated PV system could reduce cost of electricity by up to 40% [5]. Mallick et al. tested an asymmetric CPC (×2.01)-based photovoltaic module for building integration, and an increase of 62% in maximum power point was observed as compared to similar non-concentrating solar panels [6,7]. A comparative study by Yousef et al. under hot and arid climatic conditions showed that, in comparison with similar solar panels, the electricity generated by a CPC (2.4×)-based CPV system with and without cooling of solar cells was 52% and 33% higher, respectively [8]. To increase the geometric concentration and reduce the optical losses of reflective CPCs due to imperfect reflections, dielectric totally internally reflecting CPCs were tested and studied in recent years [9–12]. An experiment by Muhammad-Sukki et al. showed that the use of a mirror symmetrical dielectric CPC (4.9×) increased the power output of solar cells by a factor of 4.2 [3]. Studies by Yu et al. [13] and Baig et al. [14] showed that, for low concentrating PV systems, uneven irradiation on solar cells did not have significant effects on the CPV power output, but the incidence angle (IA) on solar cells had an significant effect when the IA is larger than 45°.

Compared to CPCs, V-trough concentrators are extremely easy to fabricate, the solar irradiation on the base of V-trough is more uniform and the unused heat is more easily dissipated through the side walls, thus making them more suitable for concentrating radiation on commercially available solar cells. Experimental studies by Sangani and Solanki showed that a V-trough concentrator (×2) increased power output by 44%, and the cost of electricity was reduced by 24% as compared to similar PV panels [15]. Solanki et al. tested a V-trough-based PV system (VPV) where the V-trough was fabricated from a single aluminum sheet, and found that the cell temperature was almost identical to that of a non-concentrated PV module [16].

Theoretical and experimental studies showed that an appropriately designed VPV was particularly adequate for water pumping due to the uniform irradiation on the solar cells [17]. A study by Bione et al. showed that the one-axis sun-tracked VPV (×2.2) increased the annual volume of pumped water by a factor of 2.49 as compared to similar fixed solar panels [18], larger than the geometric concentration of the V-trough. With an array of 1.3 kWp, Bione et al. found that the VPV water pumping system was able to irrigate 2.11 ha of grapes, but a similar fixed photovoltaic array only irrigated 1.2 ha under the climatic conditions of Petrolina, Brazil [19].

A pump directly driven by the electricity from PV modules works only when the incident radiation is above the level required to start the pump, thus to make radiation on PV panels higher than the critical level, one of best solutions is to track the Sun [20]. However, continuous sun-tracking PV systems often suffer from mechanical failures. Huang and Sun first proposed the design of a one-axis three-position sun-tracking PV system [21], and their calculations showed that the annual power output increased about 37.5% as compared to fixed PV panels in an area with abundant solar resources [22,23]. A study by Zhong et al. indicated that the annual solar gain on 3-position sun-tracked solar panels was above 96% of that collected by 2-axis tracked PV panels [24]. These studies show that one-axis 3-position sun-tracking techniques can greatly increase the power output of PV systems.

The V-trough is not an ideal solar concentrator, thus the increase of power output from VPVs is limited because, with the increase of geometric concentration (C_g) of a V-trough, more radiation is lost due to imperfect multiple reflections of solar rays on their way to the absorber [25]. To improve the optical performance of V-troughs, the reflections of solar rays on way to solar cells should be restricted, and for such VPV module (VPV-k/θ_a), all radiation within the angle θ_a is required to arrive on solar cells after less than k reflections. Similar to trough-like CPCs, the optical performance of V-troughs is uniquely determined by the projected incidence angle (θ_p) of solar rays on the cross-section of the V-trough [26–28], thus two-dimensional radiation transfer, where radiation transfer on the cross-section is considered, can reasonably predict the optical performance [28]. However, the 2-D model can't reasonably predict photovoltaic performance as the photovoltaic efficiency of solar cells is sensitive to the IA instead of θ_p [13].

In this work, a new design concept, the INSA multiple-position sun-tracked V-trough with restricted reflections (MP-VPV-k/θ_a), is proposed for potential photovoltaic water pumping applications. The design of MP-VPV-k/θ_a is that the V-trough is oriented in the north-south direction and inclined from the horizon. To ensure θ_p is always within θ_a in a day, the azimuth angle of the aperture is daily adjusted several times (M) from eastward in the morning to westward in the afternoon by rotating V-trough $2\theta_a$ about INSA once when $\theta_p = \theta_a$. To theoretically investigate the performance of MP-VPV-k/θ_a, a mathematical procedure is suggested based on the imaging principles of mirrors, solar geometry, vector algebra and three-dimensional radiation transfer with the aim to find the optimal design of such VPV for maximizing its annual electricity generation.

2. Design of MP-VPV-k/θ_a

2.1. Geometry of VPV-k/θ_a

As shown in Figure 1, according to the imaging principle of mirrors, solar rays "irradiating" on the ith left/right image of the base will arrive on the base after i reflections [25]. Therefore, when a beam of radiation is incident on the aperture of V-trough at $\theta_p \le \theta_{a,1}$, all radiation irradiating on right reflector arrives on the base after one reflection. Similarly, all radiation irradiating on the right reflector at $\theta_p \le \theta_{a,k}$ (k = 1, 2, 3 ...) arrives on the base after less than k reflections. The geometry of VPV-k/θ_a is subject to:

$$C_g = \sin[(k + 0.5)\varphi + \theta_a]/\sin(0.5\varphi + \theta_a) \quad (1)$$

where φ is the opening angle of V-trough, and the height of V-trough is $h = 0.5(C_g - 1)/\tan(0.5\varphi)$. It is known from Equation (1) that the geometric concentration C_g of VPV-k/θ_a depends on k, θ_a and φ, hence given k and θ_a, φ_g, the optimal φ for maximizing C_g, can be found. It is seen from Figure 2 that, given k, a different θ_a yields a different φ_g thus different optimal geometry of VPV-k/θ_a for maximizing C_g. As shown in Figure 3, with the increase of θ_a, C_g and h of VPV-k/θ_a optimized for maximizing C_g decrease, and φ_g increases first then decreases. It is known from Figure 3 that the φ_g varies around 30° for k = 1 and 21° for k = 2 as 8° < θ_a < 25°.

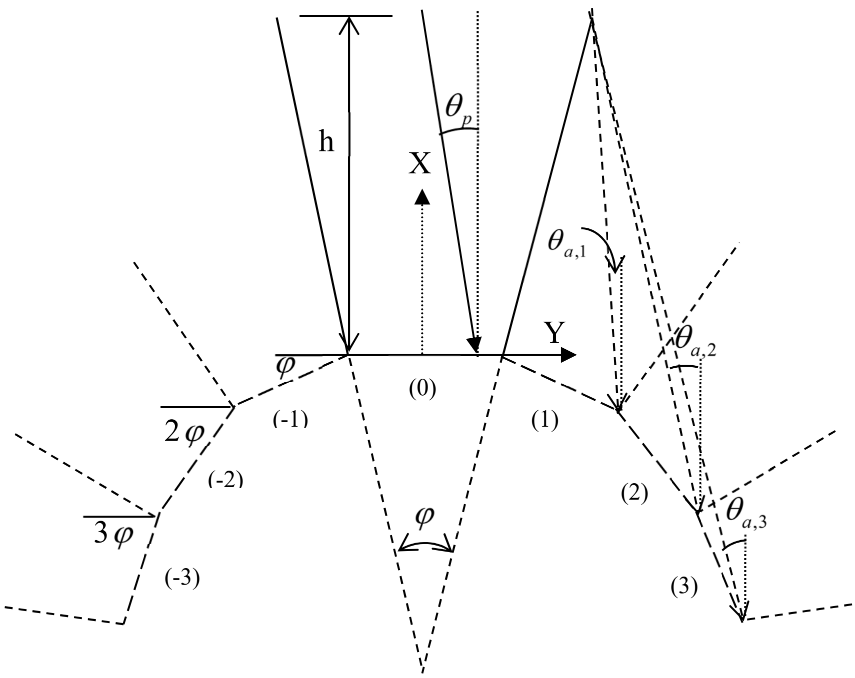

Figure 1. Consecutive images of VPV-k/θ_a.

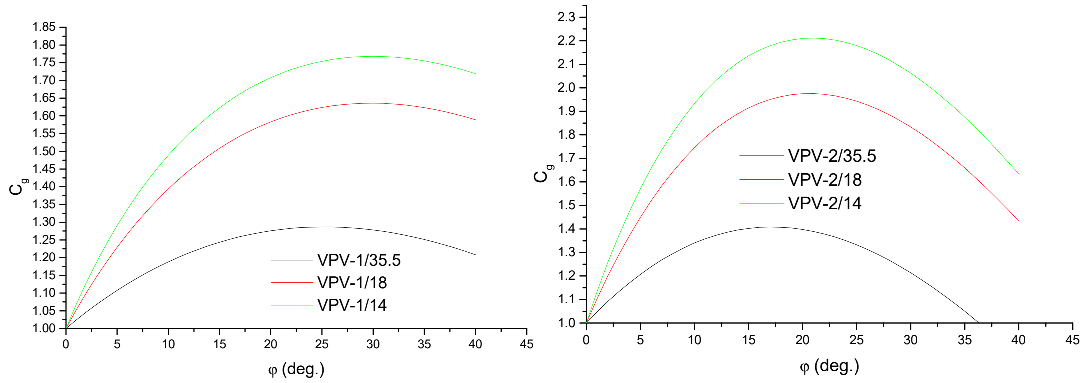

Figure 2. Effects of φ on C_g of VPV-k/θ_a.

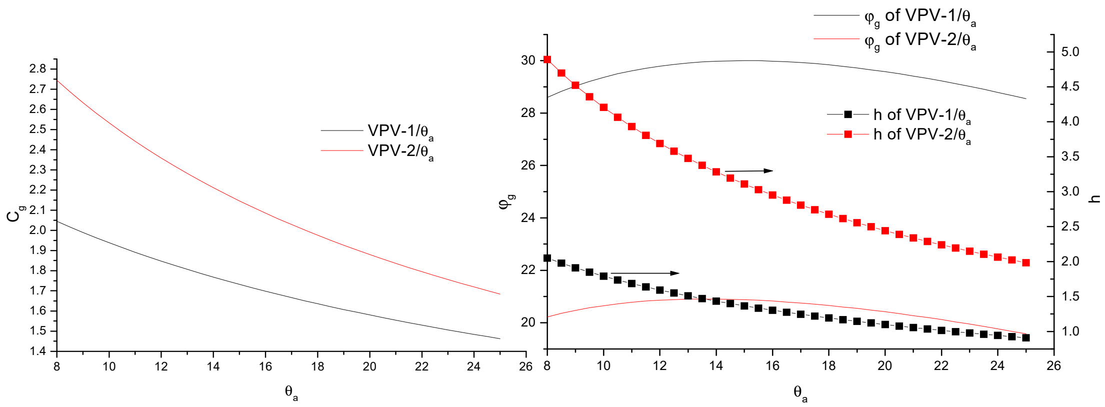

Figure 3. Effect of θ_a on C_g and ϕ_g of VPV-k/θ_a optimized for maximizing C_g.

2.2. Description of MP-VPV-k/θ_a

As shown in Figure 4, the VPV-k/θ_a is oriented in the north-south direction and inclined at β from the horizon. To make θ_p always be with θ_a in a day, a multiple-position Sun-tracking strategy is required. In the early morning, the aperture is adjusted eastward, $\gamma = (M-1)\theta_a$ from due south, then the azimuth angle is successively adjusted once when $\theta_p = \theta_a$ by rotating the V-trough $2\theta_a$ about INSA from east to west. The azimuth angle adjustment can be automatically conducted by a computerized mechanical device controlled by solar time or a photosensor.

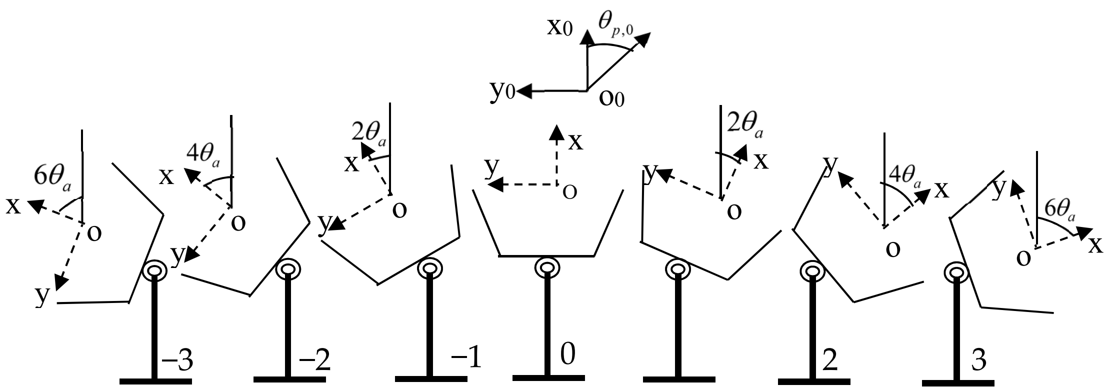

Figure 4. Back view of 7P-VPV-k/θ_a.

3. Optical and Photovoltaic Efficiency of MP-VPV-k/θ_a

3.1. Coordinate Systems Used in This Work

To be convenient for the analysis, two coordinate systems, (x_0,y_0, z_0) and (x,y,z), are employed in this work. As shown in Figure 4, both coordinate systems are fixed on the aperture of the V-trough with the x_0/x-axis normal to the aperture, and the z_0/z-axis parallel to INSA and pointing to the northern sky dome. The (x_0,y_0,z_0) system is fixed on the aperture of the V-trough at the solar-noon Sun-tracking position, thus the y_0-axis always points due east; whereas the (x,y,z) system is fixed on the aperture of the sun-tracked V-trough, thus the direction of y-axis varies during a day. In the (x_0,y_0,z_0) coordinate system, the incident solar rays at any time of a day can be expressed by a unit vector from Earth to the Sun as follows [28,29]:

$$n_{s,0} = (n_{x0}\,,\ n_{y0}\,,\ n_{z0}) \tag{2}$$

where:

$$\begin{cases} n_{x0} = \cos\delta\cos\omega\cos(\lambda-\beta)+\sin\delta\sin(\lambda-\beta) \\ n_{y0} = -\cos\delta\sin\omega \\ n_{z0} = -\cos\delta\cos\omega\sin(\lambda-\beta)+\sin\delta\cos(\lambda-\beta) \end{cases} \tag{3}$$

where λ is the site latitude, ω the solar hour angle, and δ the declination of the Sun and varies with the day number counting from first day of a year [29]. The projected angle of solar rays on the cross-section of V-trough relative to x_0-axis is given by:

$$\theta_{p,0} = \begin{cases} Atn\left|n_{y0}/n_{x0}\right| & (n_{x0} > 0) \\ 0.5\pi & (n_{x0} = 0) \\ 0.5\pi + Atn\left|n_{x0}/n_{y0}\right| & (n_{x0} < 0) \end{cases} \tag{4}$$

In the coordinate system (x, y, z), the unit vector from Earth to the Sun, n_s = (n_x, n_y, n_z), is expressed by:

$$\begin{cases} n_x = n_{x0}\cos\gamma_i - n_{y0}\sin\gamma_i \\ n_y = n_{x0}\sin\gamma_i + n_{y0}\cos\gamma_i \\ n_z = n_{z0} \end{cases} \tag{5}$$

as the coordinate system (x, y, z) is obtained by rotating the coordinate system (x_0,y_0,z_0)γ_i about z_0-axis. The γ_i in Equation (5), the azimuth angle of V-trough at the i-th Sun-tracking position relative to x_0-axis, positive in the afternoon, is determined by M, $\theta_{p,0}$ and θ_a. As an example, for 7P-VPV-k/θ_a, it is given by:

$$\gamma_i = \begin{cases} 0 & (\theta_{p,0} \le \theta_a) \\ 2\theta_a & (\theta_a < \theta_{p,0} \le 3\theta_a) \\ 4\theta_a & (3\theta_a < \theta_{p,0} \le 5\theta_a) \\ 6\theta_a & (\theta_{p,0} > 5\theta_a) \end{cases} \tag{6}$$

The optical and photovoltaic performance of VPVs for solar rays n_s = (n_x, $\pm n_y$, n_z) are identical due to the symmetric geometry, hence n_s = (n_x, $-\left|n_y\right|$, n_z) is used in this exercise for simplifying analysis, namely solar rays are always assumed to be incident onto the right reflector. The projected incident angle of solar rays on the aperture of V-trough is given by:

$$\tan\theta_p = \left|n_y/n_x\right| \text{ or } \theta_p = \left|\theta_{p,0} - \gamma_i\right| \tag{7}$$

The unit vector of normal to the horizon in the (x_0,y_0,z_0) system is expressed by:

$$n_{h,0} = (\cos\beta,\ 0,\ \sin\beta) \tag{8}$$

Also, in the (x, y, z) system, it is given based on Equation (5) as:

$$n_h = (\cos\beta\cos\gamma_i\,,\ \cos\beta\sin\gamma_i\,,\ \sin\beta) \tag{9}$$

3.2. Optical and Photovoltaic Efficiency of MP-VPV-k/θ_a

To simplify the analysis, it is assumed that the length of the V-trough is infinite as compared to the width (it is set to be 1), and side-walls are perfect specular and gray surfaces. When a beam of radiation is incident on the aperture at θ_p, a fraction of the radiation directly irradiates on the solar cells, and the remainder arrives on the solar cells after reflections from both walls. Therefore, the collectible radiation on solar cells at any time in a day includes three parts: radiation directly irradiating on the solar cells (I_1), and radiation incident on the right/left wall and arriving on solar cells after multiple reflections (I_2/I_3). Thus, the optical efficiency of the V-trough is expressed by:

$$f = (I_1 + I_2 + I_3)/I_{ap} = f_1 + f_2 + f_3 \tag{10}$$

where I_{ap} is the radiation incident on the aperture, f_1, f_2 and f_3 are the energy fractions of radiation on the solar cells contributed by I_1, I_2 and I_3, respectively. Similarly, the photovoltaic efficiency of VPVs is given by:

$$\eta = (P_1 + P_2 + P_3)/I_{ap} = \eta_1 + \eta_2 + \eta_3 \tag{11}$$

where P_i (i = 1,2,3) is the electricity generated by I_i (i = 1,2,3), and η_i is the photovoltaic efficiency contributed by P_i.

3.2.1. Calculation of f_1 and η_1

As shown in Figure 5, the base of the V-trough is fully irradiated as $\theta_p \le 0.5\varphi$, partially irradiated as $0.5\varphi < \theta_p < \theta_0$, and fully shaded by the left wall as $\theta_p \ge \theta_0$. Hence, the energy fraction of radiation directly incident on the base is given by:

$$f_1 = \frac{\Delta y_0}{A_{ap}} = \frac{\Delta y_0}{C_g}\begin{cases} 1/C_g & (\theta_p \le 0.5\varphi) \\ h(\tan\theta_0 - \tan\theta_p) & (0.5\varphi < \theta_p \le \theta_0) \\ 0 & (\theta_p > \theta_0) \end{cases} \tag{12}$$

where A_{ap} = C_g is the width of the aperture, and θ_0 (shown in Figure 5) is given by:

$$\tan\theta_0 = 0.5\left(1 + C_g\right)/h \tag{13}$$

The IA of solar rays directly irradiating on solar cells, $\theta_{in,0}$, is given by:

$$\cos\theta_{in,0} = n_s \cdot n_{base} = n_s \cdot (1,0,0) = n_x \tag{14}$$

as the vector of normal to the base is n_{base} = (1,0,0) in the system (x,y,z). Therefore, η_1 is given by:

$$\eta_1 = \Delta y_0 \eta_{pv}(\theta_{in,0})/C_g = f_1 \eta_{pv}(\theta_{in,0}) \tag{15}$$

where $\eta_{pv}(\theta_{in,0})$ is the photovoltaic efficiency of the solar cells as a function of $\theta_{in,0}$. The electricity from VPVs is commonly affected by many factors such as cell temperature, IA and solar flux distribution [14,30]. To investigate the effects of the geometry of the V-trough on power generation from VPVs, it is assumed that, except for IA, the effects of all other factors on the photovoltaic efficiency of VPVs with different geometry are identical, and the photovoltaic efficiency of solar cells is subjected to the correlation suggested by Yu et al., expressed as [13]:

$$\eta_{pv} = \begin{cases} 15.5494 + 0.023325\theta_{in} - 0.003301\theta_{in}^2 + 9.4685 \times 10^{-5}\theta_{in}^3 - 1.134 \times 10^{-6}\theta_{in}^4 & (0 < \theta_{in} < 65^\circ) \\ 41.52 - 0.47840\theta_{in} & (65^\circ \leq \theta_{in} < 90^\circ) \end{cases} \tag{16}$$

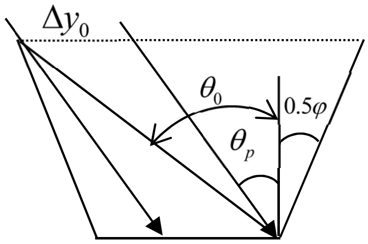

Figure 5. Radiation (Δy_0) directly irradiating on base of V-trough.

3.2.2. Calculation of f_2 and η_2

As shown in Figure 6, when solar rays are incident on the right wall of V-trough, the radiation incident on the lower part of reflector (DE) "irradiates" on the first image of base thus arrives on solar cells after one reflection, and radiation incident on the upper part of reflector (BE) "irradiates" on 2nd image hence arrives on solar cells after two reflections. Therefore, the energy fraction of radiation incident on right reflector and arriving on solar cells is given by:

$$f_2 = \sum_{k=1}^{n} \Delta y_{2,k} \rho^k / C_g \tag{17}$$

where n is the maximum reflection number of solar rays on way to solar cells, and is the integer of $90/\varphi$ or $90/\varphi - 1$ when $90/\varphi$ is an integer [25], ρ is the reflectivity of the side walls of the V-trough, and $\Delta y_{2,k}$ is the radiation "irradiating" on the kth right image and calculated based on the method given in Appendix A. The photovoltaic efficiency of VPVs due to the contribution of I_2 is calculated by:

$$\eta_2 = \sum_{k=1}^{n} \Delta y_{2,k} \eta(\theta_{in,kr}) \rho^k / C_g \tag{18}$$

where $\theta_{in,kr}$ is the IA of solar ray on the kth right image, and can be calculated by:

$$\cos\theta_{in,kr} = n_s \cdot n_{b,kr} = n_x \cos k\varphi + n_y \sin k\varphi \tag{19}$$

as the vector of normal to kth right image is $n_{b,kr}$ = (cos$k\varphi$, sin$k\varphi$, 0) in the (x,y,z) system.

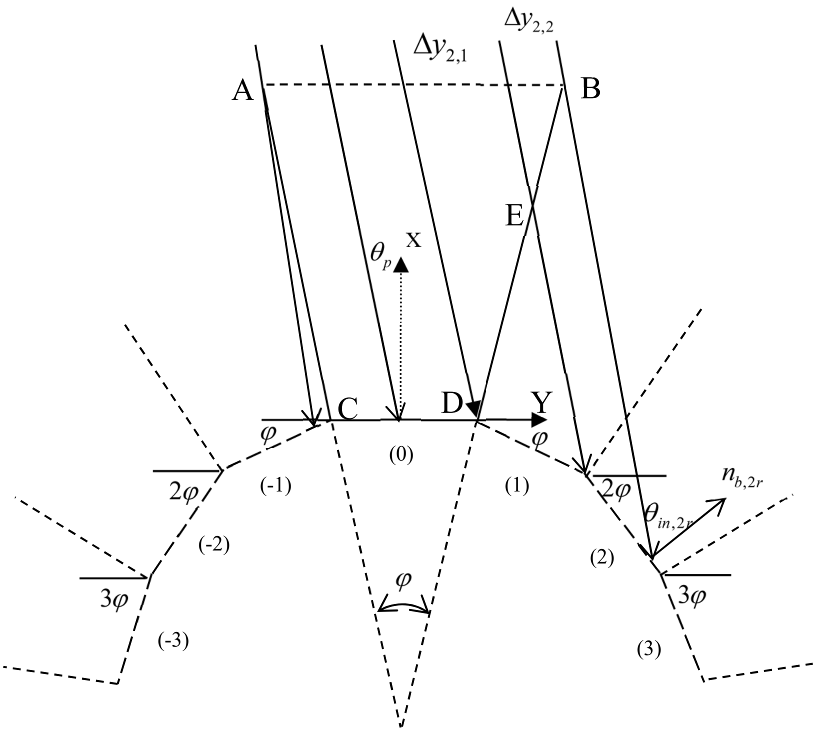

Figure 6. Radiation "irradiating" on *k*th right image of base ($\Delta y_{2,k}$).

3.2.3. Calculation of f_3 and η_3

Similarly, the energy fraction of radiation incident on the left wall of the V-trough and arriving on solar cells after multiple reflections is calculated by:

$$f_3 = \sum_{k=1}^{n} \Delta y_{3,k} \rho^k / C_g \tag{20}$$

where $\Delta y_{3,k}$ is the radiation "irradiating" on the *k*th left image, calculated based on the method given in Appendix B. The photovoltaic efficiency of VPVs due to the contribution of I_3 is calculated by:

$$\eta_3 = \sum_{k=1}^{n} \Delta y_{3,k} \eta(\theta_{in,kl}) \rho^k / C_g \tag{21}$$

where $\theta_{in,kl}$ is the IA of solar rays on the *k*th left image, and calculated by:

$$\cos\theta_{in,kl} = n_s \cdot n_{b,kl} = n_x \cos k\varphi - n_y \sin k\varphi \tag{22}$$

as the vector of normal to *k*th left image of base is $n_{b,kl}$ = (cos$k\varphi$, $-$sin$k\varphi$, 0) in the (x,y,z) system.

The analysis above shows that the f of VPVs is uniquely determined by θ_p, thus it is a function of θ_p, but the η is dependent on θ_p and the IA of solar rays on the aperture of the V-trough (θ_{ap}) since the θ_{ap} is given by cosθ_{ap} = $n_s \cdot (1, 0, 0) = n_x$.

3.3. Collectible Radiation and Power Generation of MP-VPV-k/θ_a

In the case radiation reflecting from the ground is neglected, the collectible radiation on a unit area of solar cells of MP-VPV-k/θ_a at any time of a day is calculated by:

$$I_{base} = C_g I_b g(\theta_{ap}) f \cos\theta_{ap} + I_{base,d} = C_g I_b g(\theta_{ap}) n_x f + I_{base,d} \tag{23}$$

where I_b is the intensity of the beam radiation, and $g(\theta_{ap})$ is a control function, being 1 for $\cos\theta_{ap} > 0$ and otherwise zero. The electricity generated by unit area of solar cells is expressed by:

$$P = C_g I_b g(\theta_{ap}) cos\theta_{ap}\eta + P_d = C_g I_b g(\theta_{ap}) n_x \eta + P_d \tag{24}$$

The term $I_{base,d}$ in Equation (23), the collectible sky diffuse radiation of the V-trough, is dependent on the sky dome "seen" from the aperture of MP-VPVs, and P_d in Equation (24) is the electricity generated by $I_{base,d}$. To calculate $I_{base,d}$ and P_d, it is assumed that diffuse radiation from all directions of the sky dome is identical. In the coordinate system (x,y,z), the sky diffuse radiation on a unit area of solar cells from a finite element on the sky dome (see Figure 7) is:

$$dI_{base,d} = C_g i_d \cos\theta f g(\theta_{e-h}) d\Omega \tag{25}$$

and the power generated by $dI_{base,d}$ is expressed by:

$$dP_d = C_g i_d \cos\theta \eta g(\theta_{e-h}) d\Omega \tag{26}$$

where $d\Omega = \sin\theta d\theta d\phi$ is the solid angle covered by the finite element; i_d, the directional intensity of the sky diffuse radiation, is equal to I_d/π for isotopic sky diffuse radiation [28]; and I_d is the sky diffuse radiation on the horizon. The θ_{e-h} is the IA on the horizon for sky diffuse radiation from element $d\Omega$, and $g(\theta_{e-h})$ is a control function, being 1 for $\cos\theta_{e-h} > 0$ and 0 for $\cos\theta_{e-h} < 0$ because the sky element is below the ground level in this case. The vector of sky diffuse radiation from element $d\Omega$ (see Figure 7) is expressed by:

$$n_e = (\cos\theta,\ \sin\theta\sin\phi,\ -\sin\theta\cos\phi) \tag{27}$$

Thus, the θ_{e-h} can be calculated based on n_e and n_h (given by Equation (9)) as:

$$\cos\theta_{e-h} = n_e \cdot n_h = \cos\theta\cos\beta\cos\gamma_i + \sin\theta\sin\phi\cos\beta\sin\gamma_i - \sin\theta\cos\phi\sin\beta \tag{28}$$

and the projected incident angle of sky diffuse radiation from $d\Omega$ is given by:

$$\tan\theta_p = |n_y/n_x| = |\tan\theta\sin\phi| \tag{29}$$

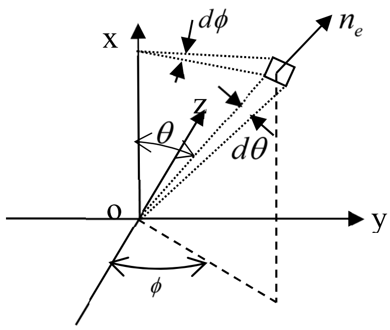

Figure 7. Vector of sky diffuse radiation from an element on the sky dome in the (x,y,z) coordinate system.

Therefore, given the geometry of MP-VPV-k/θ_a, β and γ_i, the f and η for sky diffuse radiation from finite element $d\Omega$ can be calculated, then $dI_{base,d}$ and dP_d can be calculated. The $I_{base,d}$ and P_d can be respectively calculated by integrating $dI_{base,d}$ and dP_d over the sky dome above the aperture of the V-trough as:

$$I_{base,d} = C_g i_d \iint g(\theta_{e-h}) f \sin\theta\cos\theta d\theta d\varphi = C_{d,i} I_d \tag{30}$$

$$I_{base,d}=C_g i_d \iint g(\theta_{e-h})\eta \sin\theta\cos\theta d\theta d\phi=C_{d,pv-i}I_d \tag{31}$$

where $C_{d,i}$ and $C_{d,pv-i}$ are respectively C_d and $C_{d,pv}$ for MP-VPV-k/θ_a at the ith Sun-tracking position and calculated by:

$$C_{d,i}=\frac{C_g}{\pi}\int_0^{2\pi} d\phi \int_0^{0.5\pi} g(\theta_{e-h}) f \sin\theta\cos\theta d\theta \tag{32}$$

$$C_{d,pv-i}=\frac{C_g}{\pi}\int_0^{2\pi} d\phi \int_0^{0.5\pi} g(\theta_{e-h})\eta \sin\theta\cos\theta d\theta \tag{33}$$

Given the geometry of the V-trough, β and γ_i, $C_{d,i}$ and $C_{d,pv-i}$ are constants and can be calculated by numerical calculations.

As aforementioned, the optical efficiency of linear concentrators is uniquely determined by θ_p, thus to simplify calculations of collectible sky diffuse radiation, two-dimensional isotropic sky diffuse radiation is commonly used [25,28,31]. If a 2-D sky diffuse radiation model is used, $I_{base,d}$ is calculated by:

$$I_{base,d}=C_g i_p \int_{-(0.5\pi-\gamma_i)}^{0.5\pi} f\cos\theta_p d\theta_p = C_{d,i}I_d \tag{34}$$

as θ_p varies from $-(0.5\pi-\gamma_i)$ to 0.5π for a V-trough with azimuth angle γ_i (see Figure 5). The i_p in Equation (34) is the directional intensity of sky diffuse radiation on the cross-section of the V-trough. For isotropic 2-D sky diffuse radiation, i_p can be determined by:

$$\int_{-\pi/2}^{\pi/2} i_p \cos\theta d\theta= I_{d\beta} \tag{35}$$

which leads to $i_p = 0.5I_{d\beta}$, and $I_{d\beta} = 0.5(1 + \cos\beta)I_d$ is the sky diffuse radiation on the aperture at the solar-noon Sun-tracking position. Thus $C_{d,i}$ in Equation (34) is given by:

$$C_{d,i}= 0.25C_g(1+\cos\beta)\int_{-(0.5\pi-\gamma_i)}^{0.5\pi} f\cos\theta_p d\theta_p \tag{36}$$

The daily collectible radiation on solar cells of MP-VPV-k/θ_a is estimated by integrating Equation (23) over the daytime as:

$$H_{base}=C_g\int_{-t_0}^{t_0} I_b g(\theta_{ap})n_x f dt+\int_{-t_0}^{t_0} C_{d,i}I_d dt \tag{37}$$

Daily collectible radiation on the aperture of VPVs is calculated by:

$$H_{ap}=\int_{-t_0}^{t_0} I_b g(\theta_{ap})n_x dt+\int_{-t_0}^{t_0} 0.5(1+\cos\beta\cos\gamma_i)I_d dt \tag{38}$$

as the apertures tilt angle of VPVs at the ith Sun-tracking position is given by $\cos\beta_i = n_h \cdot (1,0,0) = \cos\beta\cos\gamma_i$. The daily electricity from MP-VPVs is calculated by integrating Equation (24) over the daytime as:

$$P_{day}=C_g\int_{-t_0}^{t_0} I_b g(\theta_{ap})n_x \eta dt+\int_{-t_0}^{t_0} C_{d,pv-i}I_d dt \tag{39}$$

The daily power output from similar multiple-position Sun-tracked PV panel, $P_{day,ap}$, can be calculated based on Equations (33) and (39) by setting C_g = 1 and $\eta = \eta(\theta_{ap})$, and daily power output from similar fixed south-facing PV panels (tilted at λ) is calculated by:

$$P_{day,0}=\int_{-t_0}^{t_0} I_b g(\theta_{ap}) n_{x,0}\eta(\theta_{ap})dt+C_{d,pv-0}H_d \tag{40}$$

as the IA of solar rays on south-facing solar panels is given by $\cos\theta_{ap} = n_{x,0}$. The $C_{d,pv-0}$ is calculated by:

$$C_{d,pv-0}=\frac{1}{\pi}\int_0^{2\pi} d\phi\int_0^{0.5\pi} g(\theta_{e-h})\eta(\theta)\sin\theta\cos\theta d\theta \tag{41a}$$

$$\cos\theta_{e-h}=n_e\cdot n_{h,0}=\cos\theta\cos\lambda-\sin\theta\cos\phi\sin\lambda \tag{41b}$$

The t_0 in Equations (37)–(40) is the sunset time on the horizon. At any time of a day, the position of the Sun in terms of $n_{s,0}$ can be determined, and then f and η can be calculated. Therefore, given time variations of I_b and I_d in a day, H_{base}, H_{ap}, P_{day}, $P_{day,ap}$ and $P_{day,0}$ can be obtained by numerical calculations, then summing daily values in all days of a year gives the annual radiation on base (S_a) and aperture ($S_{a,ap}$) of the V-trough, annual power output from MP-VPVs (P_a) and similar multiple positions sun-tracked PV panels ($P_{a,ap}$) as well the annual electricity from similar fixed south-facing PV panels ($P_{a,0}$). Compared to similar multiple-position Sun-tracked PV panels, the annual collectible radiation and power output increase factors of MP-VPVs, C_s and C_p, are respectively calculated by:

$$C_s=\frac{S_a}{S_{a,ap}}=\frac{S_a}{S_{a,ap}C_g}C_g=f_aC_g \tag{42}$$

$$C_p=\frac{P_a}{P_{a,ap}}=\frac{P_a}{S_a}\times\frac{S_a}{S_{a,ap}}\times\frac{S_{a,ap}}{P_{a,ap}}=C_s\eta_a/\eta_{a,ap}=C_s=f_aC_{pv}C_g \tag{43}$$

where f_a is the annual average optical efficiency of VPVs, $\eta_a = P_a/S_a$ and $\eta_{a,ap} = P_{a,ap}/S_{a,ap}$ are the annual average photovoltaic efficiency of solar cells for concentrated and non-concentrated radiation, respectively. The $C_{pv} = \eta_a/\eta_{a,ap}$ represents the electric loss coefficient of VPVs due to increased IA on the solar cells after radiation concentration.

In the subsequent calculations, the monthly horizontal radiation averaged over many years in four sites with typical climatic conditions is used for the analysis (Beijing, λ = 39.95°, a dry area with abundant solar resources; Lhasa, λ = 29.72° in plateau with extremely abundant solar resources; Shanghai, λ = 31.2°, in a humid region; Chongqing, λ = 29.5°, poor in solar resources) [32]. The monthly average daily sky diffuse radiation on the horizon (H_d) and time variations of I_b and I_d in a day are estimated based on the correlations proposed by Collares-Pereira and Rabl [33]. The sunset time in a day is obtained based on declination of the Sun in the day. The steps of θ and ϕ for calculating $C_{d,i}$ and $C_{d,pv-i}$ are taken to be 0.1°, the interval of φ and θ_a for finding optimal design of MP-VPVs is taken to be 0.2°, and the time step to calculate the daily radiation and daily power output is set to be 1 min. To fully investigate the optimal design of MP-VPVs for maximizing P_a, 3P-, 5P- and 7P-VPVs with the tilt angle of INSA being yearly fixed (1T-MP-VPVs) and yearly adjusted four times at three tilts (3T-MP-VPVs) are addressed. For 1T-MP-VPVs, the tilt-angle β of INSA is set to be λ; whereas for 3T-MP-VPVs, β is set to be λ during periods of N days before and after both equinoxes, and adjusted to be $\lambda - \alpha$ and $\lambda + \alpha$ in summers and winters, respectively. Considering the fact that the height of VPV-k/θ_a with $k > 2$ is too large and thus not practical in applications, hence the analysis in this exercise is limited to MP-VPV-k/θ_a with k = 1 and 2.

4. Results and Discussion

4.1. Comparison of Annual Solar Gain Calculated Based on 2-D and 3-D Sky Diffuse Radiation

Figure 8 shows a comparison of $C_{d,0}$ and $C_{d,1}$ of 3P-VPV-1/20 calculated based on 2-D and 3-D sky diffuse radiation models. It shows that the 2-D model underestimates $C_{d,0}$ but overestimates $C_{d,1}$. This means that 2-D sky diffuse radiation can't reasonably estimate the collectible sky diffuse radiation of a fixed inclined north-south V-trough. However, recent work of Tang et al. [28] indicates that the 2-D model can reasonably estimate sky diffuse radiation on solar cells of east-west CPV. This is because the directional intensity of sky diffuse radiation on the cross-section of a horizontal east-west CPV is really isotropic, but not for inclined north-south V-trough or CPCs, as explained in Appendix C.

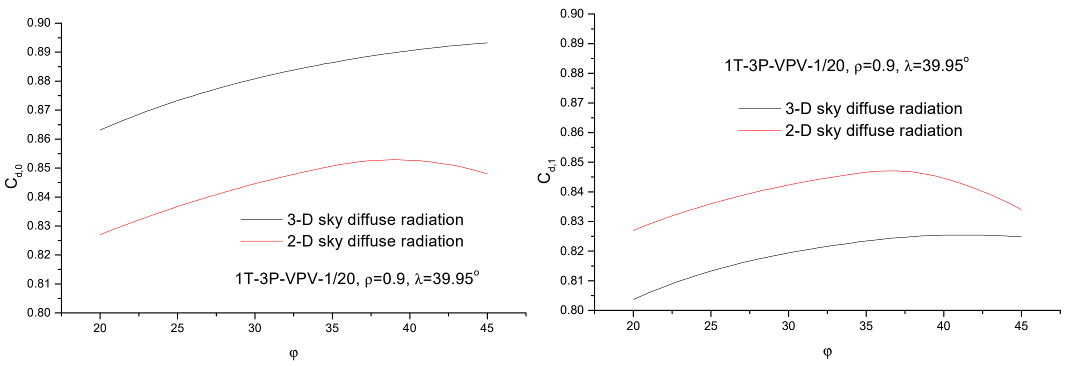

Figure 8. Comparison of $C_{d,0}$ and $C_{d,1}$ of 1T-3P-VPV-1/20 calculated based on 2-D and 3-D sky diffuse radiation.

Comparisons of annual solar gain of 1T-MP-VPVs calculated based on 2-D and 3-D sky diffuse radiation are presented in Figure 9 in terms of C_s. It is found that the difference of annual solar gain calculated based on 2-D and 3-D sky diffuse radiation is less than 0.1%, indicating that 2-D sky diffuse radiation can reasonably predict the annual solar gain of MP-VPVs although it can't predict the solar gain of fixed inclined north-south V-troughs. In the subsequent calculations, 3-D sky diffuse radiation is employed as 2-D sky diffuse radiation can't predict the photovoltaic performance of linear concentrator-based PV systems [28].

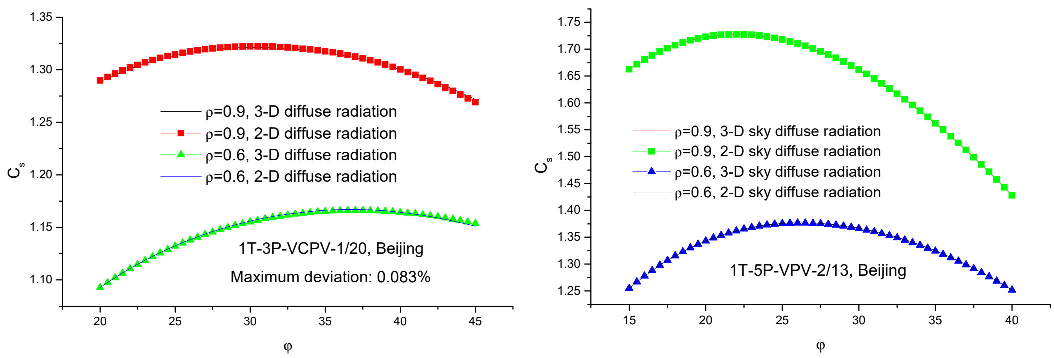

Figure 9. Comparison of annual solar gain of 1T-MP-VPVs calculated by 2-D and 3-D sky diffuse radiation.

4.2. Effects of Geometry of V-trough on the Performance of MP-VPV-k/θ_a

The analysis above shows that the annual power output of MP-VPV-k/θ_a is sensitive to M and the geometry of VPVs at a site, therefore, given M, k and θ_a, the performance of MP-VPV-k/θ_a depends on φ. As shown in Figure 10, the f_a is highly dependent on ρ. For MP-VPVs with k = 2, the f_a increases with the increase of φ as more radiation directly irradiates on the solar cells; whereas for MP-VPVs with k = 1 and high ρ, the f_a is weakly sensitive to φ because, with the increase of φ, more radiation directly irradiates on solar cells on the one hand, but in the other hand, more fraction of radiation incident on walls of the V-trough arrives on solar cells after more than one reflection.

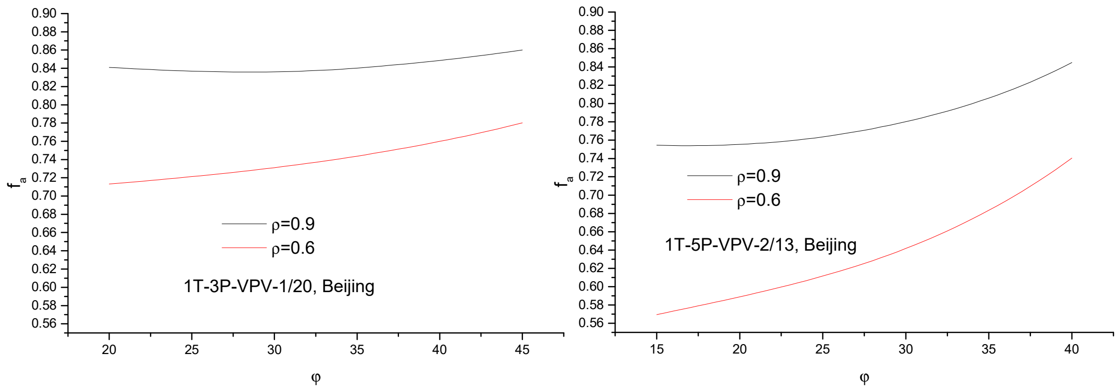

Figure 10. Effects of φ on annual average optical efficiency of 1T-MP-VPVs.

Figure 11 presents effects of φ on the photovoltaic efficiency of solar cells for radiation concentrated by MP-VPV-k/θ_a. It is seen that, for MP-VPV-k/θ_a with k = 1, the C_{pv} decreases with the increase of φ as the IA of solar rays on solar cells also increases, thus the photovoltaic efficiency decreases; whereas for MP-VPV-k/θ_a with k = 2, there is a swing because, with the increase of φ, the IA on solar cells increases on the one hand, but in the other hand, more radiation directly irradiates on the solar cells. Therefore there is a trade-off between increased optical efficiency due to more radiation directly incident on the solar cells and decreased photovoltaic efficiency of the solar cells due to increased IA. Anyway, it is seen that C_{pv} is above 0.96 for 15° $<\varphi <$ 40°, indicating that the electric loss of MP-VPV-k/θ_a due to increased IA on solar cells after radiation concentration is insignificant.

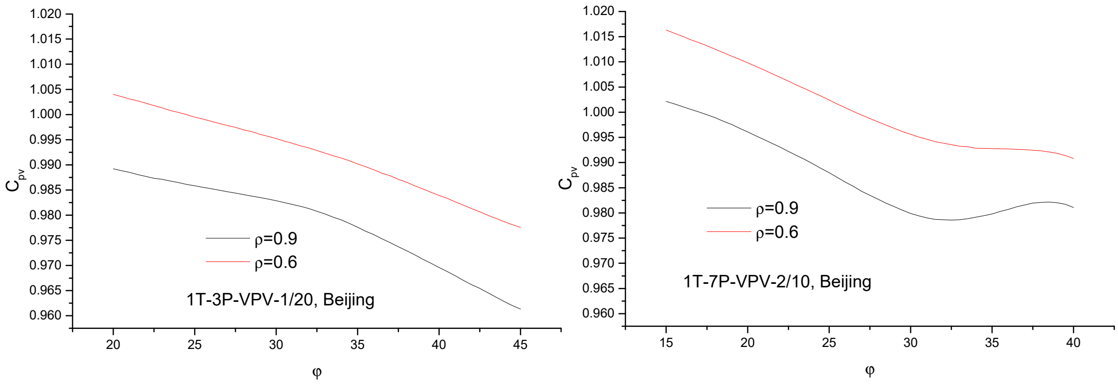

Figure 11. Effects of φ on photovoltaic efficiency of solar cells within 1T-MP-VPVs.

Effects of φ on the annual collectible radiation and electricity generation of MP-VPV-k/θ_a are presented in Figures 12 and 13. It is seen that C_s and C_p are sensitive to φ, and φ_s, the optimal φ for maximizing S_a is commonly larger than φ_p, the optimal φ for maximizing P_a. It is also found that, as compared to similar multiple positions Sun-tracked PV panels, the increase factors of annual solar gain (C_s) and power output (C_p) of MP-VPV-k/θ_a are similar but much lower than the geometric concentration since C_p = $C_{pv}C_s$ and C_{pv}≈1.

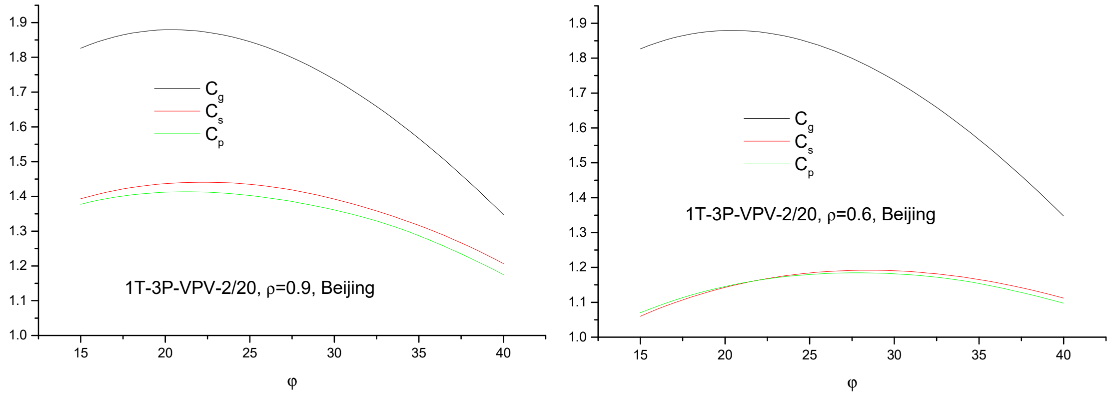

Figure 12. Effects of φ_p on annual solar gain and power output of 1T-3P-VPV-2/20.

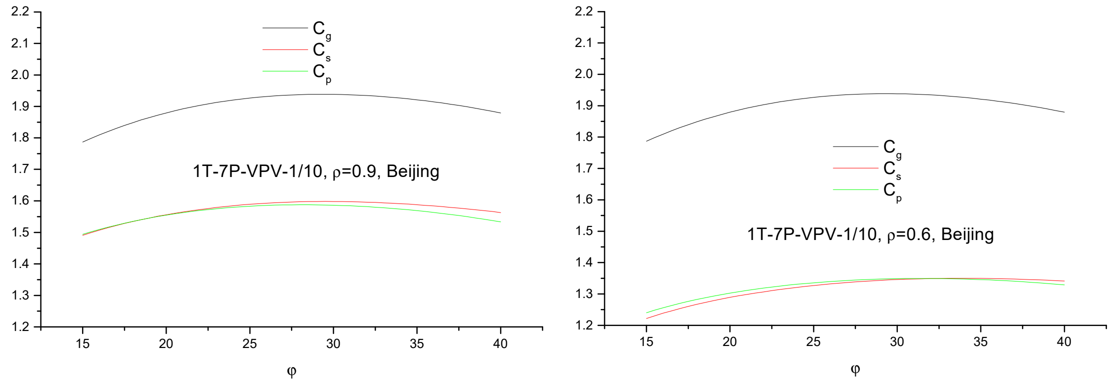

Figure 13. The same as in Figure 12 but for 1T-7P-VPV-1/10.

These results indicate that the power increase (C_p) of MP-VPV-k/θ_a being much less than C_g is mainly attributed to the optical loss due to imperfect reflections, and the electric loss due to increased IA after radiation concentration is insignificant. Results shown in Figures 12 and 13 indicate that a 3° deviation of φ from φ_p results in reduction of P_a less than 0.5%. The analysis above shows that, for a given MP-VPV-k/θ_a, an optimal φ for maximizing P_a can be found, hence different θ_a yields different φ_p thus different optimal geometry of MP-VPVs for maximizing P_a. As shown in Figure 14, given a Sun-tracking strategy (M), the maximum annual power output in terms of $C_{p,0}$, the ratio of P_a to $P_{a,0}$, is sensitive to θ_a, hence an optimal θ_a for maximizing P_a of MP-VPV-k/θ_a can be found. It is seen that, as compared to similar fixed south-facing PV panels, the annual power output increase $C_{p,0}$ of MP-VPV-k/θ_a is even larger than $C_{g,p}$, the C_g of VPVs optimized for maximizing P_a, in sites with abundant solar resources such as Beijing, but in sites with poor solar resources such as Chongqing, $C_{p,0}$ is always less than $C_{g,p}$. This implies that MP-VPV-k/θ_a is suitable to be used in sites with abundant solar resources. Calculations also indicate that 1° deviation of θ_a from the optimal value results in reduction of P_a less than 0.3%.

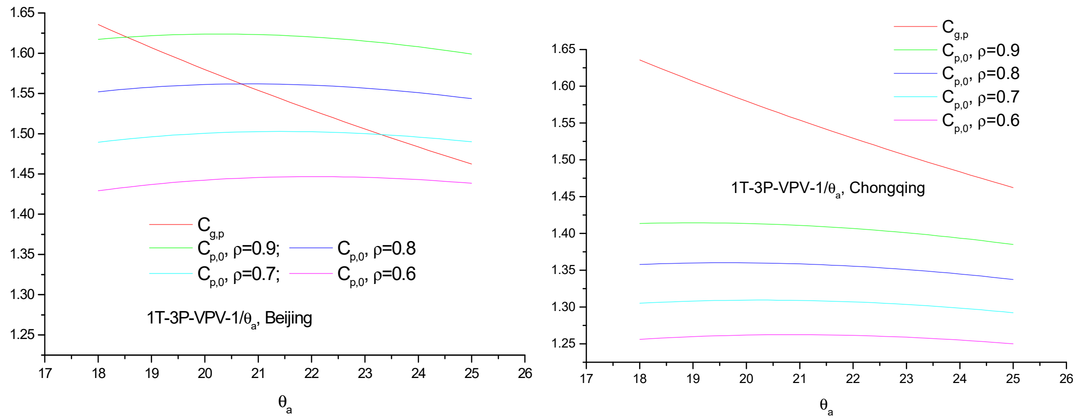

Figure 14. Effects of θ_a on maximum annual power output of 1T-3P-VPV-1/θ_a in terms of $C_{p,0}$.

4.3. Optimal Design of MP-VPV-k/θ_a for Maximizing Annual Power Output

4.3.1. Optimal Design of 1T-MP-VPV-k/θ_a

In this case, the tilt angle of INSA is fixed yearly at λ. Hence, given M, ρ and k, the P_a is dependent on θ_a and φ, thus a set of optimal θ_a and φ for maximizing P_a in a site can be found by two-loop iterative calculations. As shown in Table 1, the optimal design of 1T-3P-VPV-k/θ_a is dependent on ρ and the climatic conditions in a site. For a given site, the optimal θ_a slightly increases with the decrease of ρ. It is seen that, for k = 1, the optimal θ_a varies from 20.5° to 22° as ρ decreases from 0.9 to 0.6 except Lhasa (a site with extremely abundant solar resources) where it varies from 21.8° to 23.2° and Chongqing (a site poor in solar resources) where it varies from 19° to 21°; whereas for k = 2, the optimal θ_a is about 0.5° lower than that of similar 3P-VPV with k = 1.

Table 1. Optimal design of 1T-3P-VPV-k/θ_a for maximizing annual power output.

Site	ρ	1T-3P-VPV-1/θ_a						1T-3P-VPV-2/θ_a					
		θ_a	φ_g	φ_g	$C_{g,p}$	C_p	$C_{p,0}$	θ_a	φ_g	φ_p	$C_{g,p}$	C_p	$C_{p,0}$
Beijing	0.9	20.4	29.5	28.6	1.569	1.298	1.624	19.8	20.4	21.3	1.888	1.414	1.766
	0.8	20.8	29.4	30.3	1.559	1.247	1.562	20.4	20.4	23.2	1.849	1.328	1.661
	0.7	21.4	29.3	31.6	1.542	1.198	1.503	21	20.3	25.2	1.797	1.252	1.568
	0.6	22	29.2	33.2	1.523	1.152	1.447	21.8	20.2	27.3	1.724	1.183	1.484
Shanghai	0.9	20	29.6	29	1.58	1.269	1.513	19.4	20.5	21.7	1.905	1.368	1.63
	0.8	20.4	29.5	30.6	1.569	1.22	1.455	20.2	20.4	23.8	1.852	1.286	1.534
	0.7	21	29.4	32.4	1.55	1.173	1.401	21	20.3	26	1.784	1.214	1.449
	0.6	21.4	29.3	34.5	1.532	1.13	1.349	21.4	20.2	28.3	1.719	1.15	1.373
Lhasa	0.9	21.8	29.3	28.1	1.534	1.311	1.716	21.4	20.2	21.1	1.818	1.427	1.865
	0.8	22.2	29.2	29.5	1.525	1.261	1.652	22	20.1	22.8	1.783	1.343	1.758
	0.7	22.6	29.1	30.8	1.514	1.214	1.591	22.6	20	24.8	1.736	1.267	1.662
	0.6	23.2	29	32.2	1.497	1.168	1.532	23.2	19.9	26.6	1.681	1.2	1.575
Chongqing	0.9	19	29.7	29.6	1.607	1.237	1.415	18.4	20.6	22	1.952	1.324	1.513
	0.8	19.4	29.7	31.8	1.594	1.189	1.36	19.4	20.5	24.6	1.879	1.244	1.423
	0.7	20.2	29.6	33.8	1.567	1.145	1.309	20.2	20.4	27.2	1.797	1.175	1.344
	0.6	21	29.4	36.2	1.534	1.104	1.262	20.8	20.3	29.6	1.712	1.116	1.276

Results in Table 1 show that, for ρ > 0.8, φ_p is close to φ_g, the optimal φ for maximizing C_g; whereas for ρ < 0.8, φ_p is about 3–5° larger than φ_g. As aforementioned, 1° deviation of θ_a from the optimal value and 2–3° deviation of φ from φ_p results in the reduction of P_a by less than 0.5%. Therefore, for 1T-3P-VPV-k/θ_a (k = 1 and 2), θ_a = 21° as the optimal value is advisable except sites with extremely abundant solar resources where θ_a = 22° is recommended and sites poor in solar resources where θ_a = 20° is suggested.

Also, it is seen that, for $\rho > 0.8$, $\varphi_p = \varphi_g$ is advisable, and for $\rho < 0.8$, $\varphi_p = \varphi_g + 4°$ is recommended. Results listed Table 1 also indicate that, as compared to similar fixed PV panels, the annual power increase ($C_{p,0}$) of 3P-VPVs is higher than $C_{g,p}$ of an optimized V-trough in the sites with abundant solar resources for $\rho > 0.8$.

Optimal designs of 1T-5P-VPV-k/θ_a are presented in Table 2. It is seen that the optimal θ_a in this case for $k = 1$ and 2 are almost identical, and varies from about 13° to 14.5° as ρ decreases from 0.9 to 0.6, except at Lhasa where it varies from 13.8° to 14.8°. Therefore, $\theta_a = 13.5°$ is advisable as the optimal value except for Lhasa where $\theta_a = 14.5°$ is recommended. It is seen from Table 2 that for $k = 1$, φ_p is close to φ_g, except at Chongqing in the case of $\rho = 0.6$, hence $\varphi_p = \varphi_g$ is recommended; whereas for $k = 2$, $\varphi_p = \varphi_g$ and $\varphi_p = \varphi_g + 3°$ are advisable for $\rho > 0.8$ and $\rho < 0.8$, respectively. Similarly, it is found that, $C_{p,0}$ is also larger than $C_{g,p}$ in sites abundant in solar resources for $\rho > 0.8$.

Table 2. Optimal designs of 1T-5P-VPV-k/θ_a for maximizing annual power output.

Site	ρ	1T-5P-VPV-1/θ_a						1T-5P-VPV-2/θ_a					
		θ_a	φ_g	φ_p	$C_{g,p}$	C_p	$C_{p,0}$	θ_a	φ_g	φ_p	$C_{g,p}$	C_p	$C_{p,0}$
Beijing	0.9	13.4	29.9	28.8	1.79	1.474	1.897	13	20.9	21	2.282	1.708	2.196
	0.8	13.8	30	29.6	1.775	1.405	1.81	13.4	20.9	22.2	2.25	1.59	2.046
	0.7	14	30	30.8	1.768	1.339	1.725	13.8	20.9	23.4	2.213	1.48	1.906
	0.6	14.4	30	32	1.751	1.274	1.643	14.4	20.9	24.8	2.156	1.377	1.776
Shanghai	0.9	13	29.6	28.8	1.806	1.428	1.739	13	20.9	21.2	2.282	1.633	1.987
	0.8	13.4	29.9	30.2	1.791	1.362	1.659	13.4	20.9	22.6	2.247	1.52	1.851
	0.7	13.8	30	31.6	1.774	1.298	1.581	13.8	20.9	24	2.206	1.416	1.725
	0.6	14	30	33	1.763	1.236	1.506	14.2	20.9	25.6	2.156	1.32	1.608
Lhasa	0.9	13.8	30	28.4	1.774	1.51	2.032	14	20.9	20.8	2.211	1.753	2.362
	0.8	14.2	30	29.2	1.76	1.44	1.941	14.2	20.9	22	2.196	1.635	2.204
	0.7	14.4	30	30.2	1.753	1.373	1.851	14.6	20.9	23.2	2.161	1.524	2.056
	0.6	14.8	30	31	1.739	1.306	1.763	14.8	20.9	24.6	2.133	1.421	1.918
Chongqing	0.9	12.8	29.9	29.2	1.814	1.375	1.596	12.6	20.9	21.4	2.311	1.551	1.8
	0.8	13	29.9	31	1.806	1.312	1.523	13	20.9	23	2.273	1.443	1.676
	0.7	13.4	29.9	32.8	1.786	1.251	1.452	13.4	20.9	24.8	2.223	1.345	1.562
	0.6	13.8	30	34.6	1.764	1.193	1.385	14	20.9	26.6	2.15	1.255	1.457

Table 3 shows the optimal design of 1T-7P-VPV-k/θ_a. It is seen that, for $k = 1$, the optimal θ_a varies around 10° except for Lhasa where it varies around 10.5°, and φ_p varies around φ_g for $0.6 < \rho < 0.9$; whereas for $k = 2$, the optimal θ_a varies around 10.5° and φ_p varies near φ_g for $0.6 < \rho < 0.9$ except for Chongqing where $\theta_a = 10°$ and $\varphi_p = \varphi_g + 3°$ is recommended. To be convenient for applications, optimal designs of MP-VPV-k/θ_a recommended in this work are summarized in Table 4.

4.3.2. Optimal Design of 3T-MP-VPV-k/θ_a

In this case, the tilt-angle of INSA is adjusted yearly four times at three tilts. Therefore, given M, ρ and k, the P_a is dependent on date (N) when a tilt-angle adjustment is made, tilt-angle adjustment (α) from site latitude for each adjustment, θ_a and φ, thus a set of optimal N, α, θ_a and φ for maximizing P_a in a site can be found by multiple-loop iterative calculations. As seen from Tables 5 and 6, the optimal N is 21–22 days from equinoxes for all cases; whereas the optimal α, strongly sensitive to climatic conditions in the site and slightly to ρ, M and k, varies from 22° to 25°. Calculations show that, for a given 3T-MP-VPV-k/θ_a, one day of N from the optimal value and 2° of α from its optimal value results in reduction of P_a less than 0.1%. Hence, $N = 22$ days and $\alpha = 23.5°$ are recommended as optimal N and α, respectively. It is seen from Tables 5 and 6 that, as compared to 1T-MP-VPVs, the annual power output of 3T-MP-VPVs is about 5% higher (see the columns of $C_{p,3T\text{-}1T}$) in sites with poor solar resources and 6% in sites with abundant solar resources.

Table 3. Optimal design of 1T-7P-VPV-k/θ_a for maximizing annual power output.

Site	ρ	1T-7P-VPV-1/θ_a						1T-7P-VPV-2/θ_a					
		θ_a	φ_g	φ_p	$C_{g,p}$	C_p	$C_{p,0}$	θ_a	φ_g	φ_p	$C_{g,p}$	C_p	$C_{p,0}$
Beijing	0.9	10	29.4	28.2	1.938	1.588	2.061	9.8	20.6	20.4	2.552	1.912	2.48
	0.8	10.2	29.4	29.2	1.929	1.507	1.957	10.2	20.7	21.4	2.513	1.768	2.296
	0.7	10.4	29.5	30.2	1.919	1.427	1.855	10.4	20.7	22.4	2.489	1.633	2.122
	0.6	10.8	29.6	31.2	1.899	1.349	1.754	10.8	20.8	23.4	2.444	1.506	1.959
Shanghai	0.9	9.8	29.3	28.8	1.948	1.53	1.874	9.8	20.6	20.6	2.552	1.816	2.224
	0.8	10	29.4	29.6	1.938	1.452	1.779	10.2	20.7	21.6	2.512	1.679	2.058
	0.7	10.2	29.4	30.8	1.928	1.376	1.686	10.4	20.7	22.8	2.486	1.552	1.902
	0.6	10.4	29.5	32.2	1.915	1.302	1.595	10.6	20.7	24.2	2.452	1.432	1.755
Lhasa	0.9	10.2	29.4	28	1.928	1.635	2.222	10.4	20.7	20.4	2.495	1.979	2.691
	0.8	10.4	29.5	28.8	1.919	1.552	2.11	10.6	20.7	21.2	2.477	1.834	2.494
	0.7	10.6	29.5	29.6	1.91	1.47	2.001	10.8	20.8	22	2.456	1.696	2.309
	0.6	10.8	29.6	30.4	1.9	1.39	1.892	11	20.8	23	2.431	1.566	2.132
Chongqing	0.9	9.6	29.2	28.6	1.958	1.464	1.707	9.6	20.6	20.8	2.572	1.709	1.993
	0.8	9.8	29.3	30.2	1.948	1.389	1.62	10	20.7	22.2	2.528	1.58	1.842
	0.7	10	29.4	32	1.934	1.318	1.536	10.2	20.7	23.6	2.495	1.461	1.703
	0.6	10.2	29.4	33.8	1.918	1.248	1.455	10.6	20.7	25.2	2.435	1.349	1.573

Table 4. Recommended optimal design of MP-VPV-k/θ_a for maximizing annual power output.

VPV	ρ	VPV-1/θ_a					VPV-2/θ_a				
		θ_a	φ_g	φ_p	$C_{g,p}$	h	θ_a	φ_g	φ_p	$C_{g,p}$	h
1T-3P-	>0.8	21	29.4	29.5	1.554	1.053	21	20.3	20.5	1.836	2.311
	<0.8			33.5	1.547	0.908			24.5	1.807	1.859
1T-5P-	>0.8	13.5	29.6	29.5	1.787	1.494	13.5	20.9	21	2.246	3.362
	<0.8			29.5	1.787	1.494			24	2.227	2.887
1T-7P-	>0.8	10	29.4	29.5	1.939	1.782	10	20.7	21	2.533	4.135
	<0.8			29.5	1.939	1.782			24	2.508	3.548
3T-3P-	>0.8	20	29.6	29.5	1.581	1.102	20	20.4	20.5	1.86	2.432
	<0.8			32.5	1.576	0.988			24.5	1.852	1.963
3T-5P-	>0.8	13	29.9	30	1.806	1.505	13	20.9	21	2.282	3.459
	<0.8			30	1.806	1.505			23	2.273	3.129
3T-7P-	>0.8	9.5	29.2	29.5	1.964	1.83	10	20.7	21	2.533	4.136
	<0.8			29.5	1.964	1.83			24	2.508	3.548

Table 5. Optimal design of 3T-3P-VPV-1/θ_a for maximizing annual power output.

Sites	ρ	N	α	θ_a	φ_p	$C_{g,p}$	C_p	$C_{p,0}$	P_a	$C_{p,3T\text{-}1T}$	$P_{a,r}$
Beijing	0.9	22	24.8	19.2	29	1.602	1.322	1.727	1478.5	1.063	1477.6
	0.8	22	24.8	19.8	30.4	1.585	1.269	1.66	1421	1.063	1420.7
	0.7	22	25	20.4	31.8	1.567	1.219	1.595	1366	1.062	1365.6
	0.6	22	25	21	33.4	1.547	1.171	1.534	1313.6	1.06	1312
Shanghai	0.9	22	23	19	29.2	1.607	1.292	1.595	1096.8	1.054	1095.9
	0.8	22	23	19.6	30.8	1.59	1.241	1.533	1054.1	1.054	1053.7
	0.7	22	23.2	20.2	32.6	1.571	1.193	1.474	1013.6	1.053	1013.6
	0.6	22	23	20.6	34.2	1.554	1.148	1.418	975.1	1.051	974
Lhasa	0.9	22	25	20.4	28.6	1.569	1.341	1.823	2381.4	1.063	2380
	0.8	22	24.8	21	29.8	1.554	1.289	1.754	2290.6	1.061	2290.4
	0.7	22	24.6	21.4	31	1.543	1.238	1.687	2202.9	1.06	2201.8
	0.6	22	24.6	21.8	32.2	1.531	1.19	1.622	2118.4	1.059	2117.3
Chongqing	0.9	22	22	18.6	29.8	1.619	1.256	1.482	765	1.047	763.9
	0.8	22	22.4	19.2	31.8	1.6	1.207	1.424	735.4	1.047	734.5
	0.7	21	22.2	19.8	33.6	1.578	1.161	1.37	707.5	1.046	707.4
	0.6	21	22	20.2	35.8	1.557	1.119	1.32	681.4	1.045	680.6

Table 6. Optimal design of 3T-3P-VPV-2/θ_a for maximizing annual power output.

Sites	ρ	N	α	θ_a	φ_p	$C_{g,p}$	C_p	$C_{p,0}$	P_a	$C_{p,3T\text{-}1T}$	$P_{a,r}$
Beijing	0.9	22	24.2	18.8	21.4	1.935	1.449	1.891	1618.9	1.07	1615.7
	0.8	22	24.6	19.4	23.2	1.895	1.359	1.776	1520.8	1.069	1513.5
	0.7	22	24.8	20.4	25.2	1.824	1.278	1.673	1432.4	1.067	1432.1
	0.6	22	25	20.8	27.2	1.77	1.207	1.58	1353.3	1.065	1346.6
Shanghai	0.9	22	23.4	18.6	21.6	1.944	1.403	1.73	1189.6	1.061	1186.9
	0.8	22	23.2	19.4	23.6	1.891	1.317	1.626	1117.7	1.06	1111
	0.7	22	23.4	20	25.8	1.833	1.241	1.533	1053.8	1.058	1052.7
	0.6	22	23.2	20.6	28.2	1.756	1.174	1.45	997	1.056	989.4
Lhasa	0.9	22	25.2	20	21	1.879	1.471	1.998	2608.7	1.071	2605.6
	0.8	22	25.2	20.8	22.8	1.834	1.381	1.879	2454.3	1.069	2444.1
	0.7	22	25.2	21.4	24.6	1.788	1.301	1.773	2314.9	1.067	2314.1
	0.6	22	25.2	21.8	26.6	1.738	1.23	1.676	2189	1.064	2179.3
Chongqing	0.9	22	22.2	18	22	1.973	1.35	1.592	822	1.052	820.5
	0.8	22	22.2	18.8	24.4	1.911	1.258	1.496	772.3	1.051	766.5
	0.7	22	22.2	19.6	26.8	1.833	1.196	1.411	728.7	1.05	727.8
	0.6	22	22.6	20.4	29.4	1.735	1.134	1.338	690.8	1.048	684.4

Table 5 shows that the optimal θ_a of 3T-3P-VPV-1/θ_a varies from 19° to 21° as ρ decreases from 0.9 to 0.6 except for Lhasa, where it varies from 20.4 to 21.8°, and Chongqing, where it does so from 18.6 to 20.4°, hence, θ_a = 20° is recommend as the optimal value. It is also seen that the φ_p is about φ_g for $\rho > 0.8$ and $\varphi_g + 3$ for $\rho < 0.8$, thus $\varphi_p = \varphi_g$ and $\varphi_p = \varphi_g + 3$ are recommended for $\rho > 0.8$ and $\rho < 0.8$, respectively. As seen from Table 5, the annual power output, $P_{a,r}$, estimated based on N = 22 days, α = 23.5° as well optimal θ_a and φ_p suggested in Table 4 are almost identical to P_a of optimal 3T-3P-VPV-1/θ_a with the maximum deviation of less than 0.1%.

Optimal designs of 3T-3P-VPV-2/θ_a are given in Table 6. It indicates that, except for Lhasa and Chongqing, the optimal θ_a varies from 18.6° to 21.2°, φ_p is about φ_g for $\rho > 0.8$ and $\varphi_g + 4$ for $\rho < 0.8$. Hence, θ_a = 20° as the optimal value is advisable, and $\varphi_p = \varphi_g$ and $\varphi_p = \varphi_g + 4$ are recommended for $\rho > 0.8$ and $\rho < 0.8$, respectively. It is also seen that, the annual power output, $P_{a,r}$, calculated based on recommended optimal values of N, α, θ_a and φ_p are almost identical to those (P_a) of optimal 3T-3P-VPV-2/θ_a.

To save space, optimal designs of 3T-5P-VPV- k/θ_a and 3T-7P-VPV-k/θ_a are not presented in details, and their recommended optimal designs are presented in Table 4. It is seen from Table 4 that, with the increase of M, the θ_a decreases, but C_g and h of VPVs optimized for maximizing P_a increase. For MP-VPVs with k = 1, the $C_{g,p}$ is less than 2, and $h < 1.83$; whereas for k = 2, $1.8 < C_{g,p} < 2.53$ and $1.8 < h < 4.1$. In practical applications, one should select θ_a and M based on the requirement of C_g first, then determine φ_p based on ρ and φ_g, which is close to 30° for k = 1 and 21° for k = 2 as $8° < \theta_a < 25°$. Considering the fact that V-trough with $h > 2$ is not practical, therefore, 5P-, and 7P-VPV-2/θ_a are not advisable for applications.

5. Conclusions

Calculations and analysis show that the directional intensity of sky diffuse radiation on the cross-section of a linear concentrators is not isotropic except when the cross-section is parallel or perpendicular to the horizon, hence 2-D sky diffuse radiation can't reasonably predict collectible sky diffuse radiation of fixed inclined north-south V-troughs, but can for MP-VPVs.

Analysis shows that, at a specific site, the annual collectible radiation and power output of MP-VPV-k/θ_a is dependent on M and the geometry of VPVs. Calculations show that φ_s, the optimal φ for maximizing S_a, is commonly larger than φ_p, the optimal φ for maximizing P_a. It is also found that, as compared to similar multiple positions Sun-tracked PV panels, the increases of S_a and P_a of MP-VPV-k/θ_a are similar but much lower than C_g. Analysis shows that the power increase factor, C_p, being much less than C_g is mainly attributed to the optical loss due to imperfect reflections, and the electric loss due to increased IA of solar rays on solar cells after radiation concentration is insignificant.

Results show that, the optimal design of 1T-MP-VPV-k/θ_a for maximizing P_a is dependent on M, climatic conditions in sites and reflectivity of the side walls (ρ). The optimal θ_a is about 21°, 13.5° and 10° for 3P-, 5P- and 7P-VPVs (k = 1 and 2), respectively; whereas φ_p is about φ_g for $\rho > 0.8$ and about 3–4° larger than φ_g for $\rho < 0.8$. As compared to similar fixed south-facing PV panels, the increase of annual electricity from MP-VPV-k/θ_a is even larger than the $C_{g,p}$ of optimized MP-VPV-k/θ_a for $\rho > 0.8$ in sites with abundant solar resources.

Calculations indicate that, for 3T-MP-VPV-k/θ_a, the optimal date (N) when tilt-angle adjustment is made is about 22 days from equinoxes, and the optimal tilt adjustment from site latitude (α) for each adjustment is about 23.5°. It is found that the optimal θ_a of 3T-MP-VPV-k/θ_a is about 0.5° less than that of similar 1T-MP-VPV-k/θ_a, and φ_p is almost identical to that of similar 1T-MP-VPV-k/θ_a. As compared to similar 1T- MP-VPV-k/θ_a, the annual electricity generation from 3T-MP-VPV-k/θ_a is about 5–7% higher.

In practical applications, one should select θ_a and M based on the requirement of C_g first, then determines φ_p based on ρ and φ_g, which is about 30° for k = 1 and 21° for k = 2 as $8° < \theta_a < 25°$. However 5P-, and 7P-VPV-2/θ_a are not advisable as the height of the V-trough is more than twice the width of the base.

Author Contributions: This work is equally shared by three authors. R.T., the sponsor of the work; G.L., responsible for the development of mathematical model; J.T., student for Master, responsible for numerical calculations

Funding: This work is partial fulfillment of funded program 51466016, financially supported by National Natural Science Foundation of China.

Conflicts of Interest: The authors declare no conflict of interest.

Glossary

C_d	ratio of sky diffuse radiation on solar cells to that on the horizon (dimensionless)
$C_{d,pv}$	ratio of electricity generated by sky diffuse radiation to diffuse radiation on the horizon (dimensionless)
C_g	geometric concentration factor of V-trough (dimensionless)
$C_{g,p}$	geometric concentration of MP-VPVs optimized for maximizing annual power output (dimensionless)
C_p	annual power output increase of MP-VPVs as compared to similar sun-tracking PV panel (dimensionless)
$C_{p,0}$	annual power output increase of MP-VPVs as compared to similar fixed PV panels (dimensionless)
C_{pv}	ratio of annual average photovoltaic efficiency of solar cells for concentrated radiation to that for non-concentrating radiation (dimensionless)
C_s	annual solar gain increase of MP-VPVs as compared to similar sun-tracked solar panels (dimensionless)
f	optical efficiency of V-troughs (dimensionless)
H	daily solar gain (MJ/m^2);
h	height of V-troughs (m)
I	instantaneous radiation intensity (W/m^2)
k	reflection number allowed for radiation within θ_a
M	number of daily azimuth angle adjustment
N	days counting from equinoxes
n	unit vector of the normal to a surface
n_s	unit vector of incident solar rays
P	power output from solar cells (MJ/m^2)
S	annual collectible radiation (MJ/m^2)
t	solar time (s)

Greek letters

*α	tilt-angle adjustment of INSA from site latitude ($*$ The unit of angles is radian in mathematical expressions and degree in text)
β	tilt-angle of INSA relative to the horizon
γ_i	azimuth angle of MP-VPVs at ith sun-tracking position relative to x_0-axis
δ	declination of the sun
ϕ	azimuth angle in the spherical coordinate system
φ	opening angle of V-troughs
η	photovoltaic conversion efficiency of MP-VPVs (dimensionless)
$\eta_{pv}(\theta_{in})$	photovoltaic efficiency of solar cells as a function of θ_{in}
λ	site latitude
θ	polar angle in the spherical coordinate system
θ_a	acceptance half-angle of MP-VPVs that all incident radiation within it is required to arrive on solar cells after less than k reflections
θ_{in}	real incidence angle of solar rays on solar cells
θ_p	projected incident angle of solar rays on cross-section of V-troughs
ρ	reflectivity of side walls of V-troughs (dimensionless)
ω	hour angle

Subscripts

0	sunset; fixed PV panel
a	annual
ap	aperture
base	base of V-troughs
b	beam radiation; base
d	sky diffuse radiation
e	finite element on sky dome
day	daily
h	horizon
i	ith sun-tracking position
k	kth image of base counting from the real base of V-trough
L	left image of the base
R	right image of the base
p	power
s	sun; solar gain

Appendix A. Calculation of the Radiation "Irradiating" on *k*th Right Image of Base

$\Delta y_{2,k}$ shown in Figure 6 is given by:

$$\Delta y_{2,k} = F_R(k)\left[1 - \tan k\varphi \tan\theta_p\right] \tag{A1}$$

where $F_R(k)$ is the difference of y-coordinates between two ends of irradiated part of *kth* right image of the base, and calculated by:

$$F_R(k) = \begin{cases} 0 & Y_{e,k} - Y_{s,k} \le 0 \\ Y_{e,k} - Y_{s,k} & 0 < Y_{e,k} - Y_{s,k} \le \cos k\varphi \\ \cos k\varphi & Y_{e,k} - Y_{s,k} > \cos k\varphi \end{cases} \tag{A2}$$

The $Y_{s,k}$ is taken to be larger of $y_{s,k}$ and $R_y(k)$, and $Y_{e,k}$ is taken to be the smaller of $y_{e,k}$ and $R_y(k+1)$, namely:

$$Y_{s,k} = \mathrm{Max}\left(y_{s,k}, R_y(k)\right) \tag{A3}$$

$$Y_{e,k} = \mathrm{Min}\left(y_{e,k}, R_y(k+1)\right) \tag{A4}$$

The $y_{s,k}$ is the y-coordinate of crossing point between extended kth right image and left edge ray (the ray passing tip A), whereas $y_{e,k}$ is the y-coordinate of the crossing point between the extended kth right image and the right edge ray (the ray passing tip B). The terms $y_{s,k}$ and $y_{e,k}$ are given by:

$$y_{s,k} = \frac{R_x(k) - h + R_y(k)\tan k\varphi + 0.5C_g c\tan\theta_p}{\tan k\varphi - c\tan\theta_p} \tag{A5}$$

$$y_{e,k} = \frac{R_x(k) - h + R_y(k)\tan k\varphi - 0.5C_g c \tan\theta_p}{\tan k\varphi - c\tan\theta_p} \quad \text{(A6)}$$

in which, $R_x(k)$ and $R_y(k)$ are x-and y-coordinates of left end of kth right image, respectively, and calculated by:

$$R_x(k) = -\sum_{j=1}^{k} \sin(j-1)\varphi \ (k = 1, 2 \ldots n+1) \quad \text{(A7)}$$

$$R_y(k) = -0.5 + \sum_{j=1}^{k} \cos(j-1)\varphi \ (k = 1, 2 \ldots n+1) \quad \text{(A8)}$$

For the case of $\theta_p = 0$, $y_{s,k} = -0.5C_g$ and $y_{e,k} = 0.5C_g$ for all right images. It is noted that $\Delta y_{2,k}$ is zero, thus $f_2 = 0$ when $\theta_p > \theta_{\max}$, the maximum incidence angle with which radiation can "irradiate" on right images. The $\theta_{\max}$ is determined by:

$$\theta_{\max} = \mathrm{Max}(\theta_1, \theta_2 \ldots \theta_{n+1}) \quad \text{(A9)}$$

where θ_k is the angle of the line linking the upper tip (A) of the left reflector and the right end of the kth right image relative to the x-axis, and determined by:

$$\tan\theta_k = [R_y(k) + 0.5C_g]/[h - R_x(k)] \ (k = 1, 2 \ldots n+1) \quad \text{(A10)}$$

Appendix B. Calculation of the Radiation "Irradiating" on *k*th Left Image of Base

$\Delta y_{3,k}$, the radiation "irradiating" on kth left image of base, is given by:

$$\Delta y_{3,k} = F_L(k)[1 + \tan k\varphi \tan\theta_p] \quad \text{(A11)}$$

where $F_L(k)$ is the difference of y-coordinates between two ends of the irradiated part of the kth left image of the base, and calculated by:

$$F_L(k) = \begin{cases} 0 & L_y(k) - y_k \le 0 \\ L_y(k) - y_k & 0 < L_y(k) - y_k \le \cos k\varphi \\ \cos k\varphi & L_y(k) - y_k > \cos k\varphi \end{cases} \quad \text{(A12)}$$

In the above expression, y_k is the y-coordinate of the crossing point between the extended kth left image and the left edge ray (the ray passing tip A), and determined by:

$$y_k = \frac{h - L_x(k) + L_y(k)\tan k\varphi - 0.5C_g c \tan\theta_p}{\tan k\varphi + c\tan\theta_p} \ (k = 1, 2 \ldots n) \quad \text{(A13)}$$

For the case of $\theta_p = 0$, $y_k = -0.5C_g$ ($k = 1,2 \ldots n$). $L_x(k)$ and $L_y(k)$ in Equations (A12) and (A13) are the x-, y-coordinates of the right end of the kth left image, respectively, and calculated by:

$$L_x(k) = -\sum_{j=1}^{k} \sin(j-1)\varphi \ (k = 1, 2 \ldots n) \quad \text{(A14)}$$

$$L_y(k) = 0.5 - \sum_{j=1}^{k} \cos(j-1)\varphi \ (k = 1, 2 \ldots n) \quad \text{(A15)}$$

It is noted that, for $\theta_p > 0.5\varphi$, no radiation "irradiates" on any left images, hence $f_3 = 0$.

Appendix C.

As shown in Figure A1, i_p, the directional intensity of sky diffuse radiation on the cross-section ($X_0O_0Y_0$) of an inclined north-south V-trough, represents the sky radiation from all directions on the red-colored plane which is perpendicular to the cross-section ($X_0O_0Y_0$) and forms an angle $\theta_{p,0}$ from plane $X_0O_0Z_0$.

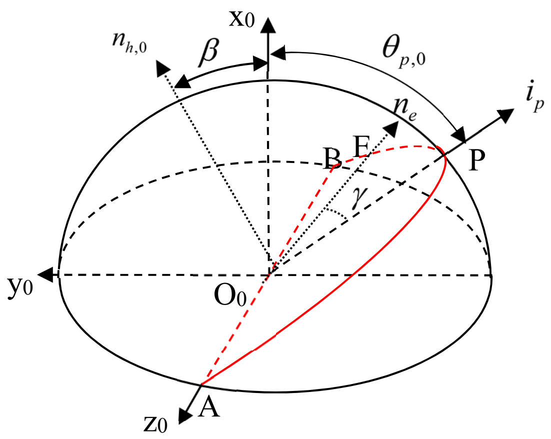

Figure A1. Directional intensity of sky diffuse radiation on cross-section of inclined north-south V-trough.

It is seen that i_p is proportional to the angle of the sky arc APE which is equal to $0.5\pi + \gamma$. The sky arc APE must be above the ground level, thus γ should be subject to $n_e \cdot n_{h,0} = 0$ which leads to:

$$\tan\gamma = \cos\theta_{p,0} / \tan\beta \tag{A16}$$

as $n_{h,0}$ = (cosβ, 0, sinβ) and n_e = (cosγcos$\theta_{p,0}$, $-$cosγsin$\theta_{p,0}$, $-$sinγ) in the coordinate system (x_0, y_0, z_0). This means that, given β, γ decreases with the increase of $\theta_{p,0}$, hence i_p decreases and is not a constant except when $\beta = 0$ or $\beta = 0.5\pi$. This indicates that, for isotropic sky diffuse radiation, the directional intensity of the sky diffuse radiation on the cross-section of linear concentrators is not isotropic except when the cross-section is perpendicular ($\beta = 0$) or parallel ($\beta = 0.5\pi$) to the horizon. Therefore, the 2-D sky diffuse radiation model can reasonably predict collectible sky diffuse radiation of horizontal east-west CPCs or V-trough as the cross-section is perpendicular to the horizon, but not for inclined north-south V-troughs or CPCs as the cross-section is not perpendicular or parallel to the horizon. This also explains why the 2-D sky diffuse radiation model underestimates $C_{d,0}$ but overestimates $C_{d,1}$ because the actual $i_p > 0.25(1 + \cos\beta)I_d$ at the solar-noon Sun-tracking position due to small $\theta_{p,0}$ but $i_p < 0.25(1 + \cos\beta)I_d$ at Sun-tracking positions in the afternoon/morning due to large $\theta_{p,0}$.

References

1. Xia, C.; Luo, H.; Tang, R.; Zhong, H. Solar thermal utilization in China. *Renew. Energy* **2004**, *29*, 1549–1556. [CrossRef]
2. Tang, R.; Yang, Y. Nocturnal reverse flow in water-in-glass evacuated tube solar water heaters. *Energy Convers. Manag.* **2014**, *80*, 173–177. [CrossRef]
3. Muhammad-Sukki, F.; Abu-Bakar, S.H.; Ramirez-Iniguez, R.; McMeekin, S.G.; Stewart, B.G.; Munir, A.B.; Yasin, S.H.M.; Rahim, R.A. Performance analysis of a mirror symmetrical dielectric totally internally reflecting concentrator for building integrated photovoltaic systems. *Appl. Energy* **2013**, *111*, 288–299.
4. Nsengiyumva, W.; Chen, S.; Hu, L.; Chen, X. Recent advancements and challenges in Solar Tracking Systems (STS): A review. *Renew. Sustain. Energy Rev.* **2018**, *81*, 250–279. [CrossRef]
5. Mallick, T.K.; Eames, P.C. Design and fabrication of low concentrating second generation PRIDE concentrator. *Sol. Energy Mater. Sol. Cells* **2007**, *91*, 597–608. [CrossRef]
6. Mallick, T.K.; Eames, P.C.; Hyde, T.J.; Norton, B. The design and experimental characterization of an asymmetric compound parabolic photovoltaic concentrator for building façade integration in the UK. *Sol. Energy* **2004**, *77*, 319–327. [CrossRef]
7. Mallick, T.K.; Eames, P.C.; Norton, B. Non-concentrating and asymmetric compound parabolic concentrating building façade integrated photovoltaic: An experimental comparison. *Sol. Energy* **2006**, *80*, 834–849. [CrossRef]
8. Yousef, M.S.; Rahman, A.K.A.; Ookawara, S. Performance investigation of low—Concentration photovoltaic systems under hot and arid conditions: Experimental and numerical results. *Energy Convers. Manag.* **2016**, *128*, 82–94. [CrossRef]
9. Su, Y.; Pei, G.; Saffa, B.R.; Huang, H. A novel lens-walled compound parabolic concentrator for photovoltaic applications. *J. Sol. Energy Eng.* **2012**, *134*, 021010. [CrossRef]

10. Li, G.; Pei, G.; Su, Y.; Ji, J.; Saffa, B.R. Experiment and simulation study on the flux distribution of lens-walled compound parabolic concentrator compared with mirror compound parabolic concentrator. *Energy* **2013**, *58*, 398–403.
11. Li, G.; Tang, J.; Tang, R. A note on design of dielectric compound parabolic concentrator. *Sol. Energy* **2018**, *171*, 500–507. [CrossRef]
12. Li, G.; Tang, J.; Tang, R. A theoretical study on performance and design optimization of linear dielectric compound parabolic concentrating photovoltaic systems. *Energies* **2018**, *11*, 2454. [CrossRef]
13. Yu, Y.; Liu, N.; Li, G.; Tang, R. Performance comparison of CPCs with and without exit angle restriction for concentrating radiation on solar cells. *Appl. Energy* **2015**, *155*, 284–293. [CrossRef]
14. Baig, H.; Sarmah, N.; Chemisana, D.; Rosell, J.; Mallick, T.K. Enhancing performance of a linear dielectric based concentrating photovoltaic system using a reflective film along the edgy. *Energy* **2014**, *73*, 177–191. [CrossRef]
15. Sangani, C.S.; Soanki, C.S. Experimental evaluation of V-trough (2 suns) PV concentrator system using commercial PV modules. *Sol. Energy Mater. Sol. Cells* **2007**, *91*, 453–459. [CrossRef]
16. Solanki, C.S.; Sangani, C.S.; Gunasheka, D.; Antony, G. Enhanced heat dissipation of v-trough PV modules for better performance. *Sol. Energy Mater. Sol. Cells* **2008**, *92*, 1634–1638. [CrossRef]
17. Vilela, O.C.; Fraidenraich, N.; Bione, J. Long term performance of water pumping systems driven by photovoltaic V-trough generators. In Proceedings of the ISES Solar World Congress 2003, Gotemborg, Sweden, 14–19 June 2003.
18. Bione, J.; Vilela, O.C.; Fraidenraich, N. Comparison of the performance of PV water pumping systems driven by fixed, tracking and V-trough generators. *Sol. Energy* **2004**, *76*, 703–711. [CrossRef]
19. Bione, J.; Vilela, O.C.; Fraidenraich, N. Simulation of grape culture irrigation with photovoltaic V-trough pumping systems. *Renew. Energy* **2004**, *29*, 1697–1705.
20. Fraidenraich, N.; Vilela, O.C. Performance of solar systems with nonlinear behavior calculated by the utilizability method. Application to PV solar pumps. *Sol. Energy* **2000**, *69*, 131–137. [CrossRef]
21. Huang, B.J.; Sun, F.S. Feasibility study of one axis three positions tracking solar PV with low concentration ratio reflector. *Energy Convers. Manag.* **2007**, *48*, 1273–1280. [CrossRef]
22. Huang, B.J.; Ding, W.L.; Huang, Y.C. Long-term test of solar PV power generation using one-axis 3-position sun tracker. *Sol. Energy* **2011**, *85*, 1935–1944. [CrossRef]
23. Gomez-Gila, F.J.; Wang, X.T.; Barnett, A. Energy production of photovoltaic systems: Fixed, tracking, and concentrating. *Renew. Sustain. Energy Rev.* **2012**, *16*, 306–313. [CrossRef]
24. Zhong, H.; Li, G.; Tang, R.; Dong, W. Optical performance of inclined south-north axis three positions tracked solar panels. *Energy* **2011**, *36*, 1171–1179. [CrossRef]
25. Tang, R.; Liu, X. Optical performance and design optimization of V-trough concentrators for photovoltaic applications. *Sol. Energy* **2011**, *85*, 2154–2166. [CrossRef]
26. Rabl, A. Comparison of solar concentrators. *Sol. Energy* **1976**, *18*, 93–111. [CrossRef]
27. Tang, R.; Wu, M.; Yu, Y.; Li, M. Optical performance of fixed east-west aligned CPCs used in China. *Renew. Energy* **2010**, *35*, 1837–1841. [CrossRef]
28. Tang, J.; Yu, Y.; Tang, R. A three-dimensional radiation transfer model to evaluate performance of compound parabolic concentrator-based photovoltaic systems. *Energies* **2018**, *11*, 896. [CrossRef]
29. Rabl, A. *Active Solar Collectors and Their Applications*; Oxford University Press: Oxford, UK, 1985.
30. Li, W.; Pau, M.C.; Sellami, N.; Sweet, T.; Montecucco, A.; Siviter, J.; Baig, H. Six-parameter electrical model for photovoltaic cell/module with compound concentrator. *Sol. Energy* **2016**, *137*, 551–563. [CrossRef]
31. Tang, R.; Wang, J. A note on multiple reflections of radiation within CPCs and its effect on calculations of energy collection. *Renew. Energy* **2013**, *57*, 490–496. [CrossRef]
32. Chen, Z.Y. *The Climatic Summarization of Yunnan*; Weather Publishing House: Beijing, China, 2001.
33. Collares-Pereira, M.; Rabl, A. The average distribution of solar radiation: Correlations between diffuse and hemispherical and between hourly and daily insolation values. *Sol. Energy* **1979**, *22*, 155–164. [CrossRef]